RESEARCH ARTICLE | NOVEMBER 08 2018

Estimation of visibility from spectral irradiance using artificial neural networks FREE

Gabriel López ✉; Christian A. Gueymard; Juan L. Bosch; Joaquín Alonso-Montesinos; Igor Rapp-Arrarás; Jesús Polo; Jesús Ballestrín; Javier Barbero; Manuel J. Caro-Parrado; Francisco J. Batlles

AIP Conf. Proc. 2033, 040023 (2018)
https://doi.org/10.1063/1.5067059

Estimation of Visibility from Spectral Irradiance Using Artificial Neural Networks

Gabriel López[1, a)], Christian A. Gueymard[2], Juan L. Bosch[1], Joaquín Alonso-Montesinos[3], Igor Rapp-Arrarás[4], Jesús Polo[5], Jesús Ballestrín[6], Javier Barbero[3], Manuel J. Caro-Parrado[1] and Francisco J. Batlles[3]

[1]*Dept. of Electrical and Thermal Engineering, Design and Projects, University of Huelva, 21004, Huelva, Spain*
[2]*Solar Consulting Services, P.O. Box 392, Colebrook, NH 03576, USA*
[3]*Dept. of Chemistry and Physics, University of Almería, 04120 Almería, Spain*
[4]*Dept. of Agricultural and Forest Science, University of Huelva, 21004, Huelva, Spain*
[5]*Photovoltaic Solar Energy Unit (Renewable Energy Division, CIEMAT), 28040 Madrid, Spain*
[6]*Concentrating Solar System Unit (Plataforma Solar de Almería, CIEMAT), 04200 Almería, Spain*

[a)]Corresponding author: gabriel.lopez@die.uhu.es

Abstract. Visibility has become a key input to determine the transmission losses of solar radiation propagating between heliostats and the receiver of solar tower power (STP) plants. Recent studies suggest that haze can reduce visibility and increase these losses up to 25% compared to clear conditions. Monitoring visibility would thus be needed for proper design and operation of STPs, but this is usually not done at all potential sites. In this work, the dependence of visibility's magnitude on relative humidity (RH) and aerosol optical depth (AOD) at three different wavelengths is analyzed. To that effect, 1-min observations from a visibilimeter located in Huelva (southwestern Spain) are analyzed during the winter season. RH is linearly correlated with visibility and explains 46% of its variability. A complex non-linear relationship between visibility and AOD is observed with also dependence on RH. Artificial neural networks (ANN) are thus investigated here for mapping the complex and non-linear relationships between visibility, RH and AOD at multiple wavelengths. This improves results significantly, increasing the explained visibility variability up to 68% and reducing RMSD from 30% to 22% with almost zero bias. The ANN analysis shows that the visibility-AOD relationship is not sensitive to the specific wavelength at which AOD is measured. These findings show that, using ANN, visibility can be estimated from local observations of RH and AOD at only a single wavelength.

INTRODUCTION

Slant-path solar transmission losses occurring between the heliostats and receiver of a solar tower power (STP) plant are mainly due to the attenuation produced by aerosols and water vapor close to the ground [1]. Whereas both the total atmospheric columns of water vapor and aerosols and their atmospheric attenuation effects are usually characterized by means of precipitable water and Aerosol Optical Depth (AOD), respectively, the modeling of slant-path attenuation typically requires additional local data, such as the slant range from heliostat to receiver or horizontal visibility at the plant [2]. Most of the existing algorithms that have been proposed in the early literature on solar transmission losses use visibility as the main input parameter to describe the aerosol load in the lower atmosphere [3, 4]. The range of possible atmospheric conditions that these models could handle was limited to two visibility values only (typically 23 km and 5 km). Such values were assumed to describe either clear conditions or hazy conditions, respectively. New studies are now being conducted to evaluate the reflected solar energy losses for a wider range of visibility values [5, 6]. The availability of maps showing how the average visibility changes over space and time (with season) would help improve the design and operation of STP plants. Unfortunately, visibility is typically only observed at airports or close to main roads, i.e. far away from STP sites. Moreover, these observations are essentially made to

SolarPACES 2017
AIP Conf. Proc. 2033, 040023-1–040023-8; https://doi.org/10.1063/1.5067059
Published by AIP Publishing. 978-0-7354-1757-1/$30.00

detect situations of very low visibility that can impair traffic safety. Most generally, the instruments used are thus not able to correctly sense high-visibility values corresponding to normal clear-sky situations. Due to this lack of direct information, the development of visibility datasets and maps requires independent estimates from other variables that are more common. One of the most important atmospheric parameters affecting visibility and its spatio-temporal variability is Relative Humidity (RH) at ground level. Humidity has a direct effect on the aerosol extinction coefficient, due to the water uptake behavior of soluble particles. This is particularly the case for rural, maritime and urban aerosols, some of which are frequent species over the study area. This RH effect in turn impacts visibility. The firsts attempt to establish a relationship between these two variables were made some 80 years ago [7]. Different functional relationships between visibility and RH have also been described in several recent studies [8, 9]. López et al. [10] have shown that visibility could be estimated with satisfactory accuracy from a number of atmospheric and broadband radiometric variables using non-linear models obtained by means of Artificial Neural Networks (ANN). Due to the visibility dependence on the amount of aerosols in the lower troposphere, a relationship between visibility and AOD is also to be expected, per Koschmieder's theoretical inverse relationship between visibility and the aerosol extinction coefficient. In this context, several experimental studies have shown the possibility to empirically derive visibility from AOD [11]. This would ultimately allow the use of satellite-based remote-sensed AOD retrievals, or results from global reanalysis models, to develop visibility maps over large areas. Such maps would become a very useful tool for the planning of new STP plants, among other applications.

Among the different terms that exist in the literature to characterize horizontal visibility, the Meteorological Optical Range (MOR) expression will be used here. Hence, the terms visibility and MOR will be used interchangeably throughout. MOR is defined by the World Meteorological Organization as the atmospheric pathlength required to reduce the luminous flux in a collimated beam from an incandescent lamp, at a colour temperature of 2700 K, to 5% of its original value. The luminous flux is evaluated by means of the photometric luminosity function of the International Commission on Illumination [12]. This definition has the advantage of being unrelated to the illuminance contrast-resolving or night-vision abilities of a human observer, and thus can be calculated by electronic devices. MOR is related to the atmospheric extinction coefficient at 550 nm, k_{ext}, using a modification of Koschmieder's Law:

$$MOR = \frac{3.00}{k_{ext}} \tag{1}$$

This extinction coefficient k_{ext} (in km^{-1}) is the sum of the Rayleigh extinction coefficient, of the gaseous absorption coefficient (in case of absorbing gases in the line of sight, such as NO_2), and of the aerosol extinction coefficient. The latter is itself proportional to AOD, at least in principle, which ultimately provides the theoretical relationship between MOR and AOD.

In this work, data from a spectroradiometer measuring direct normal spectral irradiance is used to characterize aerosols at the measurement site and to estimate visibility under cloudless conditions, in combination with RH data. In particular, the visibility's dependence on AOD is examined at three wavelengths, namely 440, 870 and 1020 nm. These specific wavelengths are purposefully selected to match those used by sunphotometers belonging to various networks, such as NASA's AERONET (AErosol RObotic NETwork). The ultimate goal here is to take advantage of that network to evaluate visibility from their observations of AOD. Whereas it is well known that visibility is an inverse function of AOD [13] and is usually impacted by high RH [11], the complex and non-linear relationships between visibility, RH and AOD have not been investigated until now. These are investigated here by means of ANNs.

DATA

The experimental setup is located at the El Arenosillo Atmospheric Sounding Station (37.1º N, 6.7º W, 40 m a.s.l.) in Huelva (southwestern Spain), a seashore site close to the Atlantic Ocean. The aerosol species that are most frequent at that station are coastal maritime, rural/continental, and desert dust [14]. The experimental dataset consists of 1-min averaged values of MOR, RH, temperature, pressure and spectral irradiance. Measurements corresponding to cloudless conditions for three months, from December 2016 to February 2017, are used in this analysis. Cloudless conditions are selected from the cloud-screened Level-1.5 dataset of one colocated Cimel sunphotometer belonging to AERONET.

Visibility is observed with a BIRAL SWS-250 sensor (Fig. 1a). This visibilimeter is a forward-scatter sensor, which measures the amount of light scattered at an angle of 45º by small particulates suspended in, or large particles passing through, its sample volume. Visibility is reported by this instrument in terms of MOR. The observable MOR

range of the BIRAL SW-250 is 10 m to 75 km, with an accuracy that is a strong function of MOR: ±5.1% at 2 km; ±12.5% at 15 km; and ≤ 20% at 30 km. Even though the specifications of such a visibilimeter announce a large range of observable visibilities, it is obvious that accurate results can only be expected under relatively hazy conditions. To put things into perspective, it is useful to relate this discussion to the intended objective of evaluating the energy losses between the mirrors and receiver of central solar tower systems. Under very clear atmospheric conditions and visibilities ranging from 50 km to more than 75 km, the variations of the energy loss are low (< 2% for mirror-to-receiver distances less than 1 km) [6]. The opposite is found for very turbid conditions: The visibilimeter is then accurate, while the variations of the energy loss may be larger than 10%.

FIGURE 1. Experimental setup at El Arenosillo (Huelva) including (a) the visibilimeter and (b) the direct normal spectroradiometer mounted on a solar tracker.

The usual meteorological variables (RH, temperature, pressure) are measured with a WS-500 sensor manufactured by Lufft GmbH. Spectral irradiance is measured with an EKO MS700 direct normal spectroradiometer mounted on an EKO automatic solar tracker, model STR-22G (Fig. 1b).

For the purpose of developing and testing the ANN models, the whole database is divided into two subsets, based on a uniformly random distribution. The training and testing data sets comprise around 1000 and 400 values, respectively. In addition, the performance results are limited to periods when visibility is below 70 km (due to the sensitivity limit of the instrument).

METHODOLOGY

In a first step, AOD is derived from spectral measurements and compared against data provided by the colocated Cimel sunphotometer. Then, an ANN is trained and validated to provide visibility from the ancillary and radiometric data inputs. The process is further described in the following subsections.

AOD Retrieval and Validation

AOD can be derived at various wavelengths from the observed direct spectral irradiance (from either the sunphotometer or the spectroradiometer) if all other sources of attenuation (e.g., Rayleigh scattering) can be accurately evaluated at those wavelengths.

TABLE 1. Statistical results of the spectroradiometer vs. sunphotometer-derived spectral irradiances.

λ [nm]	440	870	1020
RMSD [%]	2.9	2.3	2.2
MBD [%]	-1.9	1.0	-0.7

First, the measured spectral irradiance has been validated against its modeled counterpart derived from the optical depths provided by the sunphotometer measurements. These include the total optical depth, τ, which can be used to evaluate the spectral irradiance at wavelength λ from the Bouguer-Lambert-Beer law:

$$I_{n\lambda} = I_{0\lambda} E_0 e^{-\tau_\lambda m} \tag{2}$$

where E_0 is the eccentricity correction factor of the Earth's orbit and m is the air mass. Figure 2a shows the scatterplot comparing the measured to the computed spectral irradiance for various wavelengths. In addition, Table 1 provides the deviations (in terms of the root mean square deviation, RMSD, and of the mean bias deviation, MBD, both expressed in percent of the mean spectroradiometer irradiance) between the two sets of irradiance values for the same wavelengths. A satisfactory coincidence is found for all wavelengths with RMSD lower than 3% and absolute MBD values lower than 2%.

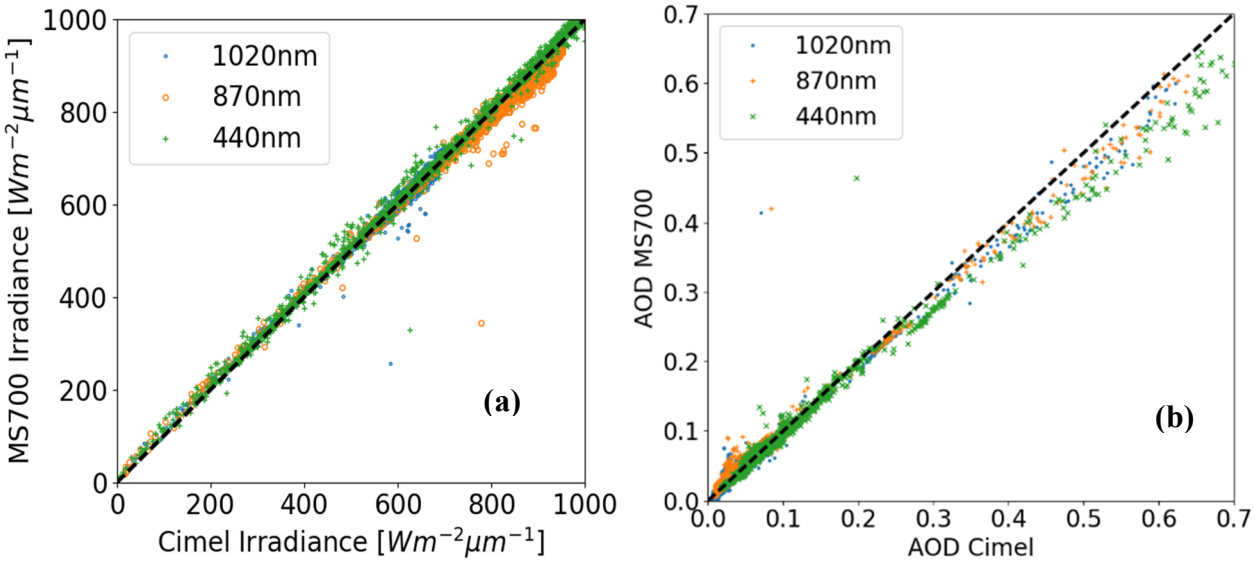

FIGURE 2. (a) Measured spectral irradiances from the spectroradiometer vs. predicted irradiance using data from the sunphotometer at three wavelengths. (b) Estimated AOD at 440, 870, and 1020 nm vs. measured values with the sunphotomer.

Additionally, the inverse process can be performed to derive total optical depths from spectral irradiances by rewriting Eq. (2) as:

$$\tau_\lambda = -Ln\left(E_0 \frac{I_{n\lambda}}{I_{0\lambda}}\right)/m \tag{3}$$

The solar irradiance has spectral windows where the only attenuation processes are caused by molecules and aerosols. This allows the derivation of AOD from the previously calculated total optical depths using:

$$AOD_\lambda = \tau_\lambda - \tau_{\lambda Ray} \tag{4}$$

where the Rayleigh optical depth, $\tau_{\lambda Ray}$, is obtained following [13]. The wavelengths at 440, 870 and 1020 nm are selected here for the AOD validation since they are essentially not affected by anything else than molecular (Rayleigh) scattering and aerosols. Figure 2b shows the computed AOD from the measured selected spectral irradiance vs. the AOD provided by the colocated sunphotometer. Both AOD estimations show a good match for values lower than 0.3, but an increasing deviation appears for higher values, mainly at 440 nm, for reason still unknown. The statistical results of the comparison of AOD derived respectively by the spectroradiometer and sunphotometer shows an average RMSD of 0.0147 and MBD of -0.0004, both in AOD unit, for the three wavelengths. Nevertheless, this comparison is only performed to check the consistency of these intermediate calculations. Further analysis would be beyond the scope of this work, but is contemplated for the near future.

Artificial Neural Network

ANNs are implemented here using a combination of custom-designed MATLAB functions [15] in conjunction with several routines developed elsewhere [16]. A standard multilayer perceptron (MLP) architecture with three fully

interconnected layers (input, hidden and output) is employed, as shown in Fig. 3. The hyperbolic tangent transform is chosen as the nonlinear activation function in the hidden layer, and the identity function is selected as the activation function for the output layer. Such a network determines a non-linear mapping from an input vector $\{x_1, x_2, ..., x_{Ni}\}$ with N_i input variables (constituted of the atmospheric and radiometric variables) to the output, i.e., MOR:

$$MOR = \sum_{j=1}^{Nh} w_j^o \tanh\left(\sum_{i=1}^{Ni+1} w_{ij}^h x_i \right) + w_{Nh+1}^o \tag{5}$$

where N_h is the number of hidden neurons, w_{ij}^h are the weights connecting the input and hidden layers and w_j^o are the weights connecting the hidden and output layers.

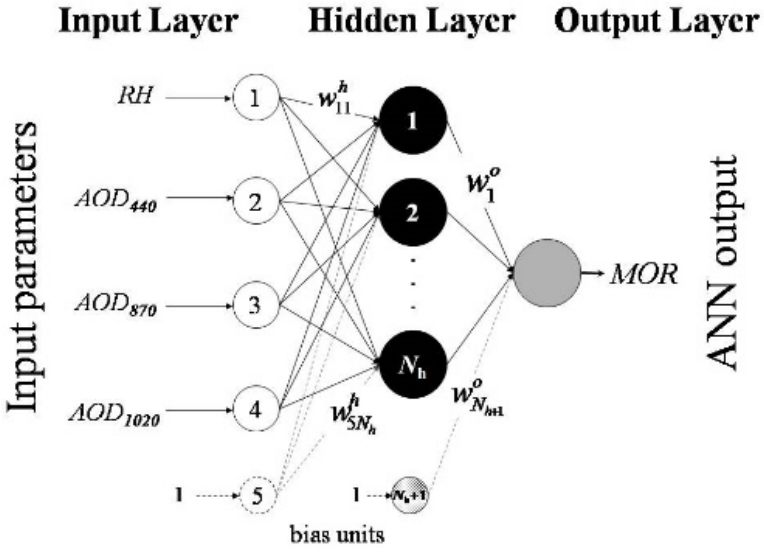

FIGURE 3. Description of the ANN architecture used here.

Whereas the number of input and output neurons is determined by the respective number of independent and dependent variables involved in the current problem, the selection of a proper value for N_h is usually not trivial. In current applications, the number of intermediate neurons is often decided in a heuristic way. In this work, the optimal number of intermediate neurons is determined empirically as the minimum number of neurons for which the performance (evaluated using the validation set) is found satisfying.

All weights are randomly initialized within the range (–0.5, 0.5). Among several existing training algorithms, a Gauss-Newton-based Levenberg-Marquartd method is selected due to its rapid convergence properties and robustness [17]. Considering the different intervals exhibited by the input and output variables, these are first normalized to have zero mean and unity variance, and then linearly scaled to remain in the interval [0.1–0.9]. This scaling is performed using the minimum and maximum values for each input and output parameter. This pre-processing of the data is only necessary in the ANN training step since the weights are back-computed afterwards to allow for raw inputs/outputs.

RESULTS

A preliminary analysis is undertaken by visual inspection of the scatterplots of MOR versus either RH or the AOD at 870 nm (AOD_{870}), expressed in the natural log scale, as Fig. 4 shows. This wavelength of 870 nm has been specifically selected to match the working wavelength (880 nm) of the BIRAL visibilimeter. A linear relationship is found with RH, albeit with significant scatter (Fig. 4a). This linear dependence has already been reported in a previous investigation, where this parameter explained ≈57% of the visibility variance [10]. In the present case, the database includes an additional month (February) with episodes of Saharan dust intrusions, causing the coefficient of determination, r^2, to decrease to 46%. A lower correlation could be expected because dust aerosols and the resulting haze are not sensitive to humidity. The scatterplot of MOR versus AOD_{870} also shows significant scatter. Nevertheless,

it seems to closely follow the type of empirical relationship proposed in [18], at least after its coefficients are revised to fit the present data. The equation displayed in Fig. 4b is able to explain about 38% of the MOR variance. The large range of visibility values when AOD is low (0.015–0.140) denotes the existence of extinction processes near ground level that cannot be fully described by AOD, since this is a columnar quantity. In a similar manner, the same MOR value may correspond to substantially different columnar amounts of aerosols. Patterns similar to Fig. 4b are also observed for the other AODs at 440 and 1020 nm. The lack of strong correlation between visibility and either RH or AOD justifies the search for a better relationship that would link visibility to both RH and AOD. This is attempted here with the goal of increasing the estimation accuracy of MOR, and ultimately that of the energy transmission losses between mirror and receiver. More generally, exploring several combinations of a number of possible input variables could be beneficial to better explain the MOR variance. This analysis is undertaken here by means of ANNs. ANNs are especially useful for nonlinear process modeling, especially in the situation where the development of the phenomenological or conventional regression models becomes impractical or cumbersome.

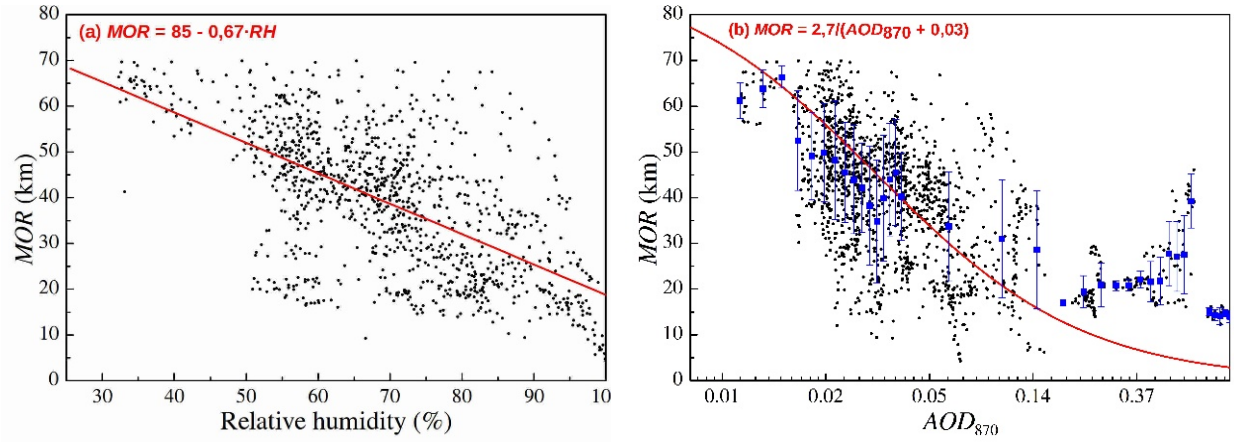

FIGURE 4. MOR versus (a) relative humidity and (b) AOD at 870 nm expressed in natural log scale. All data points corresponding to MOR ≤ 70 km are used. The best-fit equations are shown as red curves. In (b), mean values (blue squares) and standard deviations (blue lines) are shown for several intervals of AOD.

The methodology employed to define the ANN model consists firstly in calculating N_h using all input variables: RH, AOD_{440}, AOD_{870} and AOD_{1020}. This task is achieved by analyzing the ANN performance when N_h is increased from 2 to 35. The accuracy of the ANN predictions is further evaluated in terms of r^2, MBD and RMBD, resulting from the statistical analysis between estimated and measured visibilities. MBD and RMSD are calculated in percent of the mean measured visibility. For each ANN architecture (with different numbers of inputs or of hidden neurons), 10 trainings are performed. Moreover, the statistical indicators are (i) the mean of all 10 results using each statistic (r^2, MBD or RMSD), along with (ii) the corresponding standard deviation of the mean. Using this approach, local minima problems due to the random weight initializations can be avoided. The results of this first task shows that for $N_h > 3$, the ANN ensembles perform similar to each other with $r^2 = 0.68$, MBD = 0.4% and RMSD = 23%. On the other hand, using two hidden units yields an increase of RMSD, up to 28%. Based on these findings, N_h is set to 3.

The second and last step is to select the best input configuration, and to analyze the relevance of each input variable. To that end, a backward pruning is undertaken, first using all four inputs. The ANN is trained and validated ten times using the above training and test datasets. The ANN performance is analyzed based on the averaged RMSD and MBD values, along with the standard deviation corresponding to the validation data. This task is repeated using different input configurations. All cases are listed in Table 2.

Using a single AOD at only one of the three wavelengths considered here, or the combination of several AODs at different wavelengths, leads to similar visibility estimations, with RMSD values of ≈31% and overestimations (positive MBD) of ≈3%. However, these values are lower than those obtained by the equation displayed in Fig. 4b (RMSD = 37% and MBD = 5.5%), which suggests that the use of ANN provides an improvement. Nevertheless, it is difficult to establish a non-linear one-to-one relationship between visibility and AOD using either standard mathematical procedures or ANN methodology.

TABLE 2. Statistical results of the ANN performances using different input configurations. The standard deviation of the averaged RMSD and MBD is also added.

Input variables	r^2	RMSD [%]	MBD [%]
RH	0.42	30.1±0.0	0.4±0.0
AOD_{440}	0.32	31.7±0.0	3.4±0.0
AOD_{870}	0.32	31.6±0.2	3.0±0.1
AOD_{1020}	0.32	31.9±0.3	3.0±0.1
AOD_{440}, AOD_{870}, AOD_{1020}	0.35	31.1±0.1	3.3±0.1
RH, AOD_{440}	0.68	22.7±0.1	0.4±0.1
RH, AOD_{870}	0.67	23.0±0.1	0.5±0.1
RH, AOD_{440}, AOD_{870}	0.68	22.6±0.0	0.4±0.1
RH, AOD_{440}, AOD_{870}, AOD_{1020}	0.68	22.6±0.1	0.4±0.1

Remarkably, the addition of RH substantially improves the model performance, decreasing RMSD to less than 23% and consistently reducing bias (MBD = 0.4% in all cases). The overall coefficient of determination now reaches 0.68. This performance is significantly better than when either RH or AOD is used. This underlines that ANN models are able to describe the non-linear coupling between aerosols and humidity. Similarly, the present results are not sensitive to the use of either a single AOD only or a combination of several AODs at multiple wavelengths. Thus, it seems that it is sufficient to use a single AOD evaluated at a convenient wavelength along with RH measurements to estimate the horizontal visibility. Figure 5 shows the scatterplot of the ANN-estimated visibility against its measured counterpart. The data points are correctly centered along the 1:1 diagonal of perfect fit. There is some scatter for visibilities higher than 30 km, but these are within the experimental error limits assuming an uncertainty of ≈35% in the measured MOR.

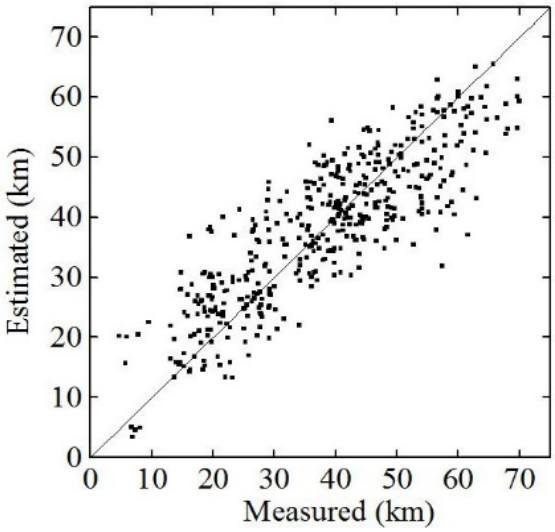

FIGURE 5. Visibility estimated using the ANN model and all input parameters vs. the measured one for the test dataset.

CONCLUSIONS

Two different methodologies based on traditional statistical techniques and artificial neural networks have been used to estimate visibility from high-frequency (1-min) observations of relative humidity and aerosol optical depth (AOD) at three different wavelengths and under cloudless skies. These AODs were calculated from spectral solar irradiance data obtained with a spectroradiometer and were found similar to those provided by a colocated sunphotometer from AERONET. The relationship between visibility and relative humidity was shown more significant than that between visibility and AOD, contrary to expectations. However, the use of ANN has revealed that visibility could be estimated with more satisfactory accuracy from the coupling of AOD, a vertically integrated

column quantity, along with the humidity at ground level. This is possible even at high (1-min) temporal resolution, despite the large variability and noise this implies. Hence, the ANN model proposed here can provide accurate visibility estimates that, in turn, are required to analyze the irradiance transmission losses throughout the heliostat-tower field of concentrating solar power plants.

Subsequent research will consider the inclusion of additional inputs, such as atmospheric pressure or wind speed, taking into account previous studies that have already underlined non-linearities in such relationships.

ACKNOWLEDGMENTS

The authors are grateful for the financial support provided by Spanish Project PRESOL (Forecast of Solar Radiation at the Receiver of a Solar Power Tower) with references ENE2014-59454-C3-2-R, ENE2014-59454-C3-1-R1 and ENE2014-59454-C3-3-R which is funded by the Ministerio de Economía y Competitividad and co-financed by the European Regional Development Fund (FEDER). The authors thank INTA-ESAt team for their assistance and for allowing the equipment to be installed in their facilities. The authors also thank the principal investigators of the El Arenosillo AERONET site: Dr. Victoria E. Cachorro and Dr. Margarita Yela.

REFERENCES

1. C.A. Gueymard, G. López and I. Rapp-Arrarás, "Atmospheric Transmission Loss in Mirror-To-Tower Slant Ranges Due to Water Vapor", AIP Conference Proceedings 1850, 140010 (2017); doi: 10.1063/1.4984518
2. J. Ballestrín and A. Marzo, Solar Energy **86**, 388–392 (2012).
3. C.N. Vittitoe and F. Biggs, "Terrestrial propagation", ASES Solar Diversification Conference Proceedings (Denver, CO, USA, 1978).
4. C.L. Pitman and L.L. Vant-Hull, "Atmospheric transmittance model for a solar beam propagating between a heliostat and a receiver", Report SAND83-8177, Sandia National Laboratories and Livermore (USA), 1984.
5. N. Hanrieder, S. Wilbert, R. Pitz-Paal, C. Emde, J. Gasteiger, B. Mayer and J. Polo, Atmos. Meas. Tech. 8, 3467–3480 (2015).
6. G. López, C.A. Gueymard and J.L. Bosch, "Evaluation of Solar Energy Losses for the Heliostat-To-Receiver Path of a Tower Solar Plant for Different Aerosol Models", SWC/SHC2017 Conference Proceedings (Abu Dhabi, UAE, 2017a).
7. H.L. Wright, Quart. J. Royal Meteorol. Soc. **65**, 411 (1939).
8. J. Chen, C.S. Zhao, N. Ma, P.F. Liu, T. Göbel, E. Hallbauer, Z.Z. Deng, L. Ran, W.Y. Xu, Z. Liang, H.J. Liu, P. Yan, X.J. Zhou, A. Wiedensohler, Atmos. Chem. Phys. **12**, 4935–4950 (2012).
9. X. Han, M. Zhang, J. Tao, L. Wang, J. Gao and S. Wang, Atmos. Env. **72**, 177–191 (2013).
10. G. López, J.L. Bosch, I. Pulido-Calvo and C.A. Gueymard, "Visibility Estimates from Atmospheric and Radiometric Variables Using Artificial Neural Networks", WIT Transactions on Ecology and The Environment **211**, 129-136 (2017b); doi:10.2495/AIR170131.
11. D. Baümer, B. Vogel, S. Versick, R. Rinke, O. Mohler and M. Schnaiter, Atmos. Env. 42, 989-998 (2008).
12. World Meteorological Organization, in *Guide to Meteorological Observing and Information Distribution Systems for Aviation Weather Services*, (WMO-No. 731, Geneva, 2014), pp. 9–16.
13. C.A. Gueymard, Solar Energy **71**, 325-346 (2001).
14. M. Sorribas, B.A. de la Morena, B. Wehner, J.F. López, N. Prats, M. Mogo, A. Wiedensohler and V.E. Cachorro, Atmos, Chem. Phys. 11, 11185-11206 (2011).
15. MatLab, The MathWorks, Inc. Natick, MA, USA, 1999.
16. M. Norgaard, "Neural network based system identification toolbox", Technical Report 97-E-851, Department of Automation, Technical University of Denmark, 1997.
17. R. Fletcher, *Practical Methods of Optimization*, (John Wiley & Sons, Chichester, 1987).
18. A. Retalis, D. G. Hadjimitsis, S. Michaelides, F. Tymvios, N. Chrysoulakis, C. R. I. Clayton and K. Themistocleous, Nat. Hazards Earth Syst. Sci. **10**, 421–428 (2010).